

# Approximate Matching of Analytic and Numerical Solutions for Rapidly Rotating Neutron Stars

Emanuele Berti<sup>1,2,3</sup> and Nikolaos Stergioulas<sup>1</sup>

<sup>1</sup> Department of Physics, Aristotle University of Thessaloniki, Thessaloniki 54124, Greece

<sup>2</sup> McDonnell Center for the Space Sciences, Department of Physics, Washington University, St. Louis, Missouri 63130, USA

<sup>3</sup> Present address: Groupe de Cosmologie et Gravitation (GReCO), Institut d'Astrophysique de Paris (CNRS), 98<sup>bis</sup> Boulevard Arago, 75014 Paris, France

29 October 2018

## ABSTRACT

We investigate the properties of a closed-form analytic solution recently found by Manko *et al.* (2000b) for the exterior spacetime of rapidly rotating neutron stars. For selected equations of state we numerically solve the full Einstein equations to determine the neutron star spacetime along constant rest mass sequences. The analytic solution is then matched to the numerical solutions by imposing the condition that the quadrupole moment of the numerical and analytic spacetimes be the same. For the analytic solution we consider, such a matching condition can be satisfied only for very rapidly rotating stars. When solutions to the matching condition exist, they belong to one of two branches. For one branch the current octupole moment of the analytic solution is very close to the current octupole moment of the numerical spacetime; the other branch is more similar to the Kerr solution. We present an extensive comparison of the radii of innermost stable circular orbits (ISCOs) obtained with a) the analytic solution, b) the Kerr metric, c) an analytic series expansion derived by Shibata and Sasaki (1998) and d) a highly accurate numerical code. In most cases where a corotating ISCO exists, the analytic solution has an accuracy consistently better than the Shibata-Sasaki expansion. The numerical code is used for tabulating the mass-quadrupole and current-octupole moments for several sequences of constant rest mass.

**Key words:** gravitation — relativity — stars: rotation — stars: neutron

## 1 INTRODUCTION

The analytic description of the vacuum spacetime surrounding a rapidly rotating neutron star is still an open problem. The analytic structure of the spacetime outside a slowly rotating star, and its relation to the Kerr metric, has been well understood since the seminal works of Hartle (1968) and Hartle & Thorne (1969). On the other hand, numerical solutions of the Einstein equations for stars rotating up to the mass-shedding limit are now routinely obtained with a number of different methods, such as the Komatsu, Eriguchi and Hachisu (1989) method (see Stergioulas 2003, for an extensive comparison of the different existing numerical methods). These numerical solutions are indeed useful for modelling astrophysical systems, for studying linear perturbations of rapidly rotating relativistic stars and as initial data for dynamical evolutions of spacetimes in numerical relativity (see e.g. Stergioulas & Friedman 1998, Stergioulas, Kluzniak & Bulik 1999, Stergioulas & Font 2001).

Despite the availability of numerical solutions, a consistent analytic representation of the vacuum metric outside a rapidly rotating neutron star is desirable for several reasons. In the first place, having an analytic form for the metric simplifies the computation of the *stationary* properties of the spacetime. For example, if an accurate analytic solution were available, geodesics in the neutron star

exterior could be studied analytically, and one could find closed-form expressions for the radii and frequencies of the innermost stable circular orbits (ISCOs). In turn, this would simplify the calculation of properties of accretion disks, of epicyclic frequencies, of accretion luminosities, and so on.

Furthermore, having an analytic solution could prove useful to the study of *dynamical* properties of the spacetime, such as gravitational wave emission. One of the unsolved problems in gravitational-wave theory is the study of the quasinormal modes of rapidly rotating neutron stars. These can be computed either in the frequency domain, as an eigenvalue problem, or in the time domain, evolving numerically the (linearized or full) Einstein equations and then computing the outgoing radiation. The major technical issue in this problem is related to the difficulty of imposing outgoing-wave boundary conditions at infinity, since a rapidly rotating neutron star spacetime is expected to deviate significantly from Petrov type D. Having in hand an accurate analytic metric for the exterior spacetime one could envisage the possibility of computing the Weyl scalars in closed form, looking for neutron star models which are, in some suitably defined sense, “close to Petrov type D” (Baker & Campanelli 2000). If the spacetime is “close enough to type D” one could then apply approximation schemes

arXiv:gr-qc/0310061v2 16 Feb 2004

to impose the outgoing-wave boundary conditions. The idea here is to improve the presently available methods, which are generally based on the use of the Zerilli functions (see e. g. Abrahams *et al.* 1992, Allen *et al.* 1998, Rupright *et al.* 1998) - i.e., on perturbations of *spherically symmetric* vacuum spacetimes. Only recently, the Teukolsky formalism for perturbations of Kerr black holes has been used for the purpose of wave extraction in the final phase of binary black holes mergers (Baker *et al.* 2002).

Until the development of a powerful integral equation method, devised by Sibgatullin in 1984 (see Sibgatullin 1991 and Manko & Sibgatullin 1993 for details), finding analytic solutions to the Einstein equations for stationary axisymmetric spacetimes was largely a matter of guesswork. One typically had to choose some ansatz to simplify the mathematical problem of obtaining the solution; then one verified *a posteriori* that the obtained solution had physically acceptable properties. In Sibgatullin's method one knows the physical characteristics of the solution to be constructed from the very beginning, through the choice of the axis expressions of the Ernst potentials.

A complete analytic representation of axisymmetric spacetimes can be obtained in terms of a series expansion whose coefficients are the physical multipole moments (Fodor, Hoenselaers & Perjés 1989, Ryan 1995). In principle, this gives an approximation to a numerical spacetime that can be made arbitrarily accurate: one would need to include a sufficiently large number of multipole moments and match them to some given numerical solution. However, such a procedure involves a very large number of expansion coefficients, which makes it difficult to use for practical purposes. Some applications of this idea have already appeared: for example, Shibata & Sasaki (1998) derived formulae for the location of the ISCO around rapidly rotating neutron stars.

Quite recently, Manko *et al.* (2000b) were able to find a new asymptotically-flat solution to the Ernst equations for the Einstein-Maxwell system. This solution is very interesting because it is given *in closed form*. Furthermore, when two of its parameters (i.e., the charge and magnetic moment) are set to zero, the solution depends only on *three parameters*: mass, angular momentum and a third parameter  $b$ , which is related to the spacetime's physical quadrupole moment. With this simplification, the solution reduces to a particular three-parameter specialization of the Kinnersley-Chitre (1978) solution (a generalization of the Tomimatsu-Sato  $\delta = 2$  spacetime). Notice however that Kinnersley and Chitre only constructed the relevant Ernst potential (they did not provide explicit expressions for the corresponding metric functions). Furthermore, the Kinnersley-Chitre solution is restricted to the subextreme case ( $M^2 > a^2$ ). On the other hand, in the solution by Manko *et al.*, when electric and magnetic fields are set to zero  $M$  and  $a$  are allowed to assume arbitrary real values, because the parameter set in their solution is analytically extended. Therefore the Kinnersley-Chitre solution is obtained as a particular case of the analytic solution in Manko *et al.* (2000b) when certain restrictions are imposed on the parameters of that solution.

There have been attempts in the literature to fix the free parameters in analytic exterior solutions by matching them to numerical solutions. However, different matching conditions were used. For example, Sibgatullin & Sunyaev (1998, 2000) fixed the free parameters appearing in a different analytic solution using the radii of marginally stable circular orbits, or a suitably defined redshift parameter at the stellar equator. For their metric, which is different from the one we consider here, they found that corrections due to the quadrupole moment can accurately reproduce the properties of the "exact" exterior spacetime only for several equations of state

(EOSs), with the exception of EOSs with large phase transitions. A simple, closed form expression for the analytic metric used in Sibgatullin & Sunyaev (1998, 2000) was given explicitly by Sibgatullin (2002).

A matching procedure based on the redshift parameter was again used by Stute & Camenzind (2002). Our own preference here is to avoid matching using *local* properties and, instead, match the solution's mass-quadrupole moment, which is a *global* property of the spacetime. Furthermore, it is well known that deviations from the slow-rotation behavior in rapidly rotating stars, due to the stellar oblateness, are determined mainly by the mass-quadrupole moment. The quadrupole moment was also used in matching the analytic and numerical solution in Manko *et al.* (2000a).

The plan of the paper is as follows. In section 2 we describe the procedure to numerically compute the spacetime describing a rapidly rotating compact star using the Komatsu-Eriguchi-Hachisu (1989) self-consistent field method, as modified by Cook, Shapiro and Teukolsky (1994, henceforth CST). In particular, we discuss how to implement this method for a numerical evaluation of the spacetime's multipole moments. In section 3 we present the analytic solution recently obtained by Manko *et al.* (which is only valid in the vacuum prevailing outside the rotating neutron star) and describe its multipolar structure. In section 4 we describe our procedure to match Manko's analytic solution to the numerically obtained spacetime, and derive the coordinate transformation relating the two metrics. Section 5 is devoted to a discussion of the tests we used in order to understand "how close" the analytic and numerical spacetimes are. As we will discuss in the following, there are two possible families of analytic solution for which the mass-quadrupole moment of the analytic solution matches to the mass-quadrupole moment of the numerical spacetime. The current-octupole moment of the first family of solutions is very close to the current-octupole moment of the numerical spacetime, while the second solution is close to the Kerr spacetime. An examination of the metric functions on the equatorial plane and on the rotation axis confirms that the first solution is also the one which better approximates the numerically obtained metric functions. As an independent check, we compute the location of ISCOs in the spacetime surrounding the rotating star using different approaches. In particular we locate ISCOs using the analytic solution, and compare the results thus obtained: 1) to the ISCOs found by numerical integration of the Einstein equations, and 2) to the analytic formulae for the ISCO's obtained by Shibata & Sasaki (1998), truncated at different orders of approximation. In most cases where a corotating ISCO exists, the analytic solution has an accuracy consistently better than the Shibata-Sasaki expansion. Only in some cases the higher-order multipoles that are missing in the analytic solution significantly increase the error in computing the location of the ISCO. Finally, we compare our matching procedure to previous work by Manko *et al.* (2000a) and by Stute & Camenzind. The conclusions follow.

## 2 NUMERICAL GRAVITATIONAL FIELD OF A RAPIDLY ROTATING NEUTRON STAR

To begin with, in this section we briefly discuss the procedure for obtaining highly-accurate numerical solutions for the spacetime of rapidly rotating neutron stars and for computing their multipole moments. For more details the reader is referred to the review article by Stergioulas (2003).

## 2.1 Numerical determination of the spacetime and computation of the multipole moments

The interior and exterior spacetime of a stationary, axisymmetric star is described by a metric in the following form:

$$ds^2 = -e^{2\nu} dt^2 + B^2 e^{-2\nu} r^2 \sin^2 \theta (d\phi - \omega dt)^2 + e^{2\alpha} (dr^2 + r^2 d\theta^2), \quad (1)$$

where  $\nu$ ,  $B$ ,  $\alpha$  and  $\omega$  are four metric functions to be determined by solving four field equations. In the numerical method of Komatsu *et al.* (1989, henceforth KEH) one defines two auxiliary functions  $\bar{\rho}$ ,  $\bar{\gamma}$  through the relations  $\nu = (\bar{\gamma} + \bar{\rho})/2$  and  $B = e^{\bar{\gamma}}$ . Then, three out of the four field equations are written in the following integral forms

$$\begin{aligned} \bar{\rho}(r, \mu) = & - \sum_{n=0}^{\infty} e^{-\bar{\gamma}/2} \\ & \left\{ \int_0^{\infty} dr' \int_0^1 d\mu' r'^2 f_{2n}^2(r, r') P_{2n}(\mu') S_{\bar{\rho}}(r', \mu') \right\} \\ & P_{2n}(\mu), \end{aligned} \quad (2)$$

$$\begin{aligned} \bar{\gamma}(r, \mu) = & - \frac{2}{\pi r \sin \theta} \sum_{n=1}^{\infty} e^{-\bar{\gamma}/2} \\ & \left\{ \int_0^{\infty} dr' \int_0^1 d\mu' r'^2 \frac{f_{2n-1}^2(r, r') \sin[(2n-1)\theta']}{2n-1} S_{\bar{\gamma}}(r', \mu') \right\} \\ & \sin[(2n-1)\theta], \end{aligned} \quad (3)$$

$$\begin{aligned} \omega(r, \mu) = & - \frac{1}{r \sin \theta} \sum_{n=1}^{\infty} e^{(2\bar{\rho}-\bar{\gamma})/2} \\ & \left\{ \int_0^{\infty} dr' \int_0^1 d\mu' r'^3 \frac{\sin \theta' f_{2n-1}^2(r, r')}{2n(2n-1)} P_{2n-1}^1(\mu') S_{\omega}(r', \mu') \right\} \\ & P_{2n-1}^1(\mu), \end{aligned} \quad (4)$$

where

$$\begin{aligned} f_n^1(r, r') &= \left(\frac{r'}{r}\right)^n \quad \text{for } r' \leq r, \\ f_n^1(r, r') &= \left(\frac{r}{r'}\right)^n \quad \text{for } r' > r, \\ f_n^2(r, r') &= \frac{1}{r} \left(\frac{r'}{r}\right)^n \quad \text{for } r' \leq r, \\ f_n^2(r, r') &= \frac{1}{r} \left(\frac{r}{r'}\right)^n \quad \text{for } r' > r, \end{aligned}$$

and  $S_{\bar{\rho}}$ ,  $S_{\bar{\gamma}}$  and  $S_{\omega}$  are lengthy source terms, whose expressions can be found in KEH. In the equations above,  $\mu = \cos \theta$ , while  $P_n(\mu)$  denotes the Legendre polynomials and  $P_n^m(\mu)$  the associated Legendre functions. The metric function  $\alpha$  is determined by an ordinary differential equation.

We compute numerical equilibrium models using the code by Stergioulas and Friedman (1995) (see Nozawa *et al.* 1998 and Stergioulas 2003 for extensive accuracy tests). The numerical code uses the CST formulation, in which the KEH equations are written in terms of a compactified coordinate  $s$  defined through the relation

$$r = r_e \left( \frac{s}{1-s} \right), \quad (5)$$

where  $r_e$  is the (coordinate) radius of the stellar equator. This allows the computation of the whole exterior spacetime out to infinity, which is important in detailed comparisons of the numerical metric to the analytic metric.

For a configuration that is stationary, axisymmetric, symmetric with respect to reflections in the equatorial plane and asymptotically flat, the spacetime can be characterized by two sets of scalar multipole moments: the even-valued mass moments ( $M_0, M_2, M_4 \dots$ ) and the odd-valued current moments ( $S_1, S_3, S_5 \dots$ ). Ryan (1997) presented a method for extracting the multipole moments from the asymptotic form of the metric functions. The lowest-order appearance of each moment in terms of a power series in  $1/r$  is determined by the expansions

$$\bar{\rho} = \sum_{n=0}^{\infty} -2 \frac{M_{2n}}{r^{2n+1}} P_{2n}(\mu), \quad (6)$$

and

$$\omega = \sum_{n=1}^{\infty} \frac{-2}{2n-1} \frac{S_{2n-1}}{r^{2n+1}} \frac{P_{2n-1}^1(\mu)}{\sin \theta}. \quad (7)$$

By comparison with equations (2) and (4) one finds that

$$M_{2n} = \frac{1}{2} \int_0^{\infty} dr' \int_0^1 d\mu' r'^{2n+2} P_{2n}(\mu') S_{\bar{\rho}}(r', \mu'), \quad (8)$$

and

$$S_{2n-1} = \frac{1}{4n} \int_0^{\infty} dr' \int_0^1 d\mu' r'^{2n+2} \sin \theta' P_{2n-1}^1(\mu') S_{\omega}(r', \mu'). \quad (9)$$

Thus, in general, any model of a rapidly rotating neutron star has an infinite number of mass- and current-multipole moments. In order to match an analytic exterior metric to a numerically-computed interior metric and to check the accuracy of the matching procedure, we computed the mass-quadrupole moment  $M_2$  and the current-octupole moment  $S_3$ .

An alternative, asymptotic method for evaluating the multipole moments was introduced by Laarakkers & Poisson (1997). We also used their method in order to cross-check the results obtained from the integral relations (8) and (9). The idea, in this case, is to evaluate numerically the coefficient of  $P_{2n}(\mu)$  in the general expression for (2) - or analogously, the coefficient of  $P_{2n-1}^1(\mu)$  in (4) - at the outermost grid points (i.e., as  $r \rightarrow \infty$ ), and multiply the result by the appropriate factor (containing powers of  $r$ ) that can be obtained from equations (6) and (7). We have checked that the two methods typically agree to better than one part in  $10^3$ .

## 2.2 Equilibrium sequences

The equilibrium solutions for a given EOS form a two-parameter family. In particular, *stable* equilibrium solutions are bounded by four limit sequences. These limits are shown in Figure 1, which displays the gravitational mass  $M$  vs. the central energy density  $\epsilon_c$  for one the EOSs derived by Akmal, Pandharipande and Ravenhall (1998, henceforth APR). As an illustrative example we consider the APR EOS which does not include boost interactions (we refer to the original paper for details). The qualitative picture does not change when we consider other EOSs (see eg. CST, where plots are presented for a representative sample of EOSs). The solid line is the *static* limit - that is, the sequence of nonrotating solutions to the standard Tolman-Oppenheimer-Volkoff equations. The long-dashed line is the *mass-shedding* (Kepler) limit, which is determined by the condition that the centrifugal force exactly balances the gravitational attraction at the stellar equator, in which case a fluid element on the equator has the same angular velocity as a free particle in a Keplerian orbit at the same location. Both sequences terminate at high central density at the *stability* limit, where equilibrium solutions are marginally stable to axisymmetric perturba-

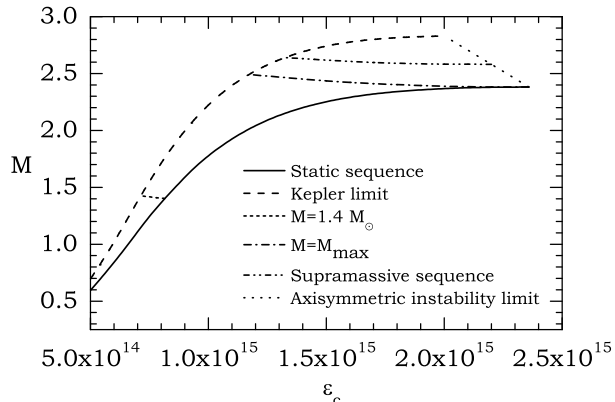


**Figure 1.** Limit sequences for EOS APR: the solid line corresponds to the nonrotating limit; the long-dashed line corresponds to the mass-shedding (Kepler) limit; the dotted line is the axisymmetric instability limit. The nearly horizontal lines are sequences of constant rest mass. From bottom to top: the dashed line corresponds to a star of gravitational mass  $M = 1.4M_\odot$  in the non rotating limit; the dash-dot line is a maximum-mass normal sequence; and finally, the dash-dot-dot line is a selected supramassive sequence.

tions; and they terminate at low central densities at the *low-mass* limit, below which a neutron star cannot form (not shown in Figure 1).

Within the class of stable equilibrium solutions, CST pointed out the significance of constant rest-mass sequences, called *evolutionary sequences*, since an isolated neutron star, slowly losing energy and angular momentum via some dissipative process (e.g. electromagnetic emission or gravitational-wave radiation), must evolve conserving the total baryon number, and hence its rest mass  $M_B$ . An accreting neutron star in a binary system will not evolve along a constant rest-mass sequence: the actual sequence depends on several parameters, such as the magnetic field, accretion rate etc. Nevertheless, the constant rest-mass sequences in CST have been used in the past in evaluating the accuracy of analytic exterior solutions and we will also use them here solely for the same reason. We compute three constant rest-mass sequences for each EOS:

- the sequence corresponding to a canonical neutron star having gravitational mass  $M = 1.4M_\odot$  in the non rotating limit,
- the sequence terminating at the maximum-mass model in the non rotating limit (maximum-mass normal sequence).
- a supramassive sequence, i.e., a sequence which does not terminate at a nonrotating model.

We include the following set of EOSs. For comparison with CST we include EOSs A, AU, FPS and L. We refer to their paper for an extensive discussion of each EOS. We supplement the set of EOSs considered by CST with a relatively new model: the model derived by Akmal, Pandharipande and Ravenhall (1998) from Hamiltonian many-body theories of nuclear matter, including boost corrections in the Hamiltonian (henceforth, we will refer to this model as APR-b, where “b” stands for “boosted”).

In Tables (1–5) we give numerical results for the structure properties of the models we have computed. All models have been computed using a resolution of (301 angular points)  $\times$  (601 radial points), corresponding to a typical accuracy of at least one part in  $10^3$  in all quantities. Each Table corresponds to a constant rest mass sequence, and lists: the total central energy density  $\epsilon_c$  in units of  $10^{15} \text{ g cm}^{-3}$ ; the angular velocity  $\Omega$  in units of  $10^3 \text{ s}^{-1}$ ; the mo-

ment of inertia  $I$  in units of  $10^{45} \text{ g cm}^2$  (for rotating models only); the gravitational mass  $M$  in solar masses; the ratio of rotational kinetic energy to gravitational binding energy  $T/W$ ; the equatorial circumferential radius of the star  $R_e$  in km and the height (in km) of corotating ( $h_+$ ) and counterrotating ( $h_-$ ) ISCOs from the surface of the star (if an ISCO does not exist, the corresponding entry is omitted). The height of an ISCO is defined as the difference between the circumferential radius at the ISCO and the circumferential equatorial radius of the star. The next three columns give the first few physical multipoles in geometrized units of  $c = G = 1$ : namely, we list the mass quadrupole moment  $M_2 \equiv Q$  in  $\text{km}^3$ , the angular momentum  $S_1 \equiv J$  in  $\text{km}^2$ , and the current octupole moment  $S_3$  in  $\text{km}^4$ . We have checked our code by reproducing the quadrupole moments computed by Laarakkers & Poisson and found excellent agreement. The accuracy in computing  $S_3$  was checked by comparing the integral form to the asymptotic form mentioned in Section 2.1, finding good agreement. This shows that using the compactified coordinate introduced in CST allows a very accurate numerical determination of relatively high-order multipoles.

The last column gives the value of the “quadrupole” parameter  $b$  (in km) for which the analytic solution provides a good approximation of the numerical spacetime. When matching the quadrupole moment of the numerical and analytic spacetimes is not possible, the corresponding entry is omitted. More details on the procedure we followed to obtain the values listed in this column will be given in section 4.

### 3 ANALYTIC GRAVITATIONAL FIELD OF A RAPIDLY ROTATING NEUTRON STAR

In this section we summarize the properties of the vacuum analytic solution obtained by Manko *et al.* (2000b). We will concentrate in particular on the multipolar structure of the solution, since our ultimate purpose will be to reproduce accurately the first few multipoles of the numerical spacetimes we discussed in the previous section.

#### 3.1 The solution by Manko *et al.*

In the vacuum region surrounding a stationary and axisymmetric star, the spacetime only depends on three metric functions (while four metric functions are needed for the interior). The most general form of the metric (Papapetrou 1953) is

$$ds^2 = -f(dt - w d\phi)^2 + f^{-1} \left\{ e^{2\gamma} (d\tilde{\rho}^2 + d\tilde{z}^2) + \tilde{\rho}^2 d\phi^2 \right\}. \quad (10)$$

Here  $f$ ,  $w$  and  $\gamma$  are functions of the quasi-cylindrical Weyl-Lewis-Papapetrou coordinates  $(\tilde{\rho}, \tilde{z})$ . Starting from this metric one can write down the vacuum Einstein-Maxwell equations as two equations for two complex potentials  $\mathcal{E}$  and  $\Phi$ , following a procedure due to Ernst (1968). The equations are:

$$(\text{Re}\{\mathcal{E}\} + |\Phi|^2) \nabla^2 \mathcal{E} = (\nabla \mathcal{E} + 2\Phi^* \nabla \Phi) \cdot \nabla \mathcal{E} \quad (11)$$

$$(\text{Re}\{\mathcal{E}\} + |\Phi|^2) \nabla^2 \Phi = (\nabla \mathcal{E} + 2\Phi^* \nabla \Phi) \cdot \nabla \Phi \quad (12)$$

Once the potentials are known, the metric can be reconstructed. Sibgatullin (1991) devised a powerful procedure for reducing the solution of the Ernst equations to simple integral equations. Basically, one starts with a choice for the values of the Ernst potentials on the symmetry axis

$$e(\tilde{z}) \equiv \mathcal{E}(\tilde{\rho} = 0, \tilde{z}), \quad f(\tilde{z}) \equiv \Phi(\tilde{\rho} = 0, \tilde{z}), \quad (13)$$

solves two complex-valued integral equations, and checks that the obtained solution satisfies the expression of the Ernst potentials in terms of physical multipoles:

$$\mathcal{E} = \frac{1-\xi}{1+\xi}, \quad \Phi = \frac{q}{1+\xi} \quad (14)$$

$$\xi(\tilde{\rho} = 0) = \sum_{n=0}^{\infty} m_n \tilde{z}^{-(n+1)}, \quad (15)$$

$$q(\tilde{\rho} = 0) = \sum_{n=0}^{\infty} q_n \tilde{z}^{-(n+1)} \quad (16)$$

The real parts of  $m_n$  are the mass multipoles, the imaginary parts of  $m_n$  are the current multipoles, the real parts of  $q_n$  are the electric multipoles and the imaginary parts of  $q_n$  are the magnetic multipoles.

After more than ten years of work in the field, Manko *et al.* (2000b) were finally able to find a vacuum solution involving five parameters (mass, angular momentum, charge, magnetic dipole moment and mass quadrupole moment) which can be expressed in terms of relatively simple rational functions. We are particularly interested in solutions having no charge or magnetic dipole moment. If we denote by  $M$  the gravitational mass of the star, by  $a$  the specific angular momentum ( $a = J/M$ ), and introduce a parameter  $b$  which can be related to the mass quadrupole moment, their choice for the axis values of the Ernst potentials is:

$$e(z) = \frac{(z-M-ia)(z+ib)+d-\delta-ab}{(z+M-ia)(z+ib)+d-\delta-ab}, \quad f(z) = 0 \quad (17)$$

with

$$\delta = \frac{-M^2 b^2}{M^2 - (a-b)^2}, \quad (18)$$

$$d = \frac{1}{4} [M^2 - (a-b)^2]. \quad (19)$$

To be able to write the metric in rational form, one must introduce generalized spheroidal coordinates

$$x = \frac{r_+ + r_-}{2k}, \quad y = \frac{r_+ - r_-}{2k}, \quad (20)$$

where  $r_{\pm} = \sqrt{\tilde{\rho}^2 + (\tilde{z} \pm k)^2}$  and

$$k = \sqrt{d + \delta}. \quad (21)$$

The inverse transformation between the two sets of coordinates is

$$\tilde{\rho} = k(1-y^2)^{1/2}(x^2-1)^{1/2}, \quad \tilde{z} = kxy. \quad (22)$$

The metric is then written as

$$ds^2 = f(dt - w d\phi)^2 - \frac{k^2}{f} \left[ e^{2\gamma} (x^2 - y^2) \left( \frac{dx^2}{x^2 - 1} + \frac{dy^2}{1 - y^2} \right) + (x^2 - 1)(1 - y^2) d\phi^2 \right], \quad (23)$$

with

$$f = \frac{E}{D}, \quad e^{2\gamma} = \frac{E}{16k^8(x^2 - y^2)^4}, \quad w = \frac{-(1-y^2)F}{E}, \quad (24)$$

and

$$\begin{aligned} D = & \{4(k^2 x^2 - \delta y^2)^2 + 2kmx[2k^2(x^2 - 1) \\ & + (2\delta + ab - b^2)(1 - y^2)] \\ & + (a-b)[(a-b)(d-\delta) - m^2 b](y^4 - 1) - 4d^2\}^2 \\ & + 4y^2\{2k^2(x^2 - 1)[kx(a-b) - mb] - 2mb\delta(1 - y^2) \end{aligned}$$

$$+ [(a-b)(d-\delta) - m^2 b](2kx+m)(1-y^2)\}^2 \quad (25)$$

$$\begin{aligned} E = & \{4[k^2(x^2 - 1) + \delta(1 - y^2)]^2 \\ & + (a-b)[(a-b)(d-\delta) - m^2 b](1 - y^2)^2\}^2 \\ & - 16k^2(x^2 - 1)(1 - y^2)\{(a-b)[k^2(x^2 - y^2) + 2\delta y^2] \\ & + m^2 b y^2\}^2 \end{aligned} \quad (26)$$

$$\begin{aligned} F = & 8k^2(x^2 - 1)\{(a-b)[k^2(x^2 - y^2) + 2\delta y^2] + y^2 m^2 b\} \\ & \times \{kmx[(2kx+m)^2 - 2y^2(2\delta + ab - b^2) - a^2 + b^2] \\ & - 2y^2(4\delta d - m^2 b^2)\} + \{4[k^2(x^2 - 1) + \delta(1 - y^2)]^2 \\ & + (a-b)[(a-b)(d-\delta) - m^2 b](1 - y^2)^2\} \\ & \times (4(2kmbx + 2m^2 b)[k^2(x^2 - 1) + \delta(1 - y^2)] \\ & + (1 - y^2)\{(a-b)(m^2 b^2 - 4\delta d) \\ & - (4kmx + 2m^2)[(a-b)(d-\delta) - m^2 b]\}). \end{aligned} \quad (27)$$

In order for the solution to satisfy the requirements of axisymmetry, stationarity and reflection-symmetry in the equatorial plane, all three parameters  $M$ ,  $a$  and  $b$  must be real.

### 3.2 Multipolar structure of the analytic solution

Here we examine the multipolar structure of the analytic solution by Manko *et al.* for rotating and nonrotating solutions. The only nonvanishing multipole moments of the solution are the gravitational mass  $Re\{m_0\} \equiv M$ , the quadrupole moment  $Re\{m_2\} \equiv Q$ , the angular momentum  $Im\{m_1\} \equiv J = aM$  and the current octupole  $Im\{m_3\} = S_3$ . The quadrupole moment and the current octupole moment are given in terms of the three parameters  $M$ ,  $a$  and  $b$  as

$$Q = -M(d - \delta - ab + a^2), \quad (28)$$

and

$$S_3 = -M \left\{ a^3 - 2a^2 b + a \left[ b^2 + 2(d - \delta) \right] - b(d - \delta) \right\}. \quad (29)$$

However, since  $a$  and  $b$  are independent parameters, setting  $a$  equal to zero does not automatically imply a vanishing  $Q$  and  $S_3$ , as would be the case for a realistic solution of a nonrotating perfect fluid star. Instead, the nonrotating solution ( $a = 0$ ) has a quadrupole moment equal to

$$Q(a = 0) = -\frac{M(M^2 + b^2)^2}{4(M^2 - b^2)}, \quad (30)$$

and a current octupole moment equal to

$$S_3(a = 0) = -bQ(a = 0). \quad (31)$$

It is obvious that there exists no real value of the parameter  $b$  for which the quadrupole moment vanishes for a nonrotating star. For  $|b| < M$ , the solution is oblate ( $Q < 0$ ) with a minimum quadrupole deformation obtained for  $b = 0$

$$|Q|_{\min}(a = 0) = M^3/4. \quad (32)$$

At  $b = \pm M$ , the nonrotating multipole moments  $Q$  and  $S_3$  diverge, while for  $|b| > M$ , the nonrotating solution is prolate ( $Q > 0$ ) with a minimum quadrupole deformation of

$$Q_{\min}(a = 0) = 2M^3, \quad (33)$$

at  $b = \pm\sqrt{3}M$ .

Obviously, the analytic solution by Manko *et al.* does not reduce continuously to the Schwarzschild solution as the rotation

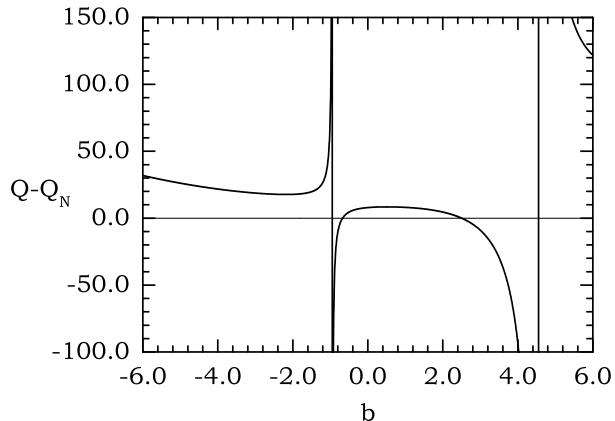


**Figure 2.** The matching condition  $Q - Q_N = 0$  as a function of  $b$  for the fastest rotating FPS model in the maximum-mass sequence (last row of  $M_B = 2.105M_\odot$  sequence in Table 3). There are two possible solutions: a solution for which (typically, as in the case shown)  $b = b_- < 0$ , and a positive solution for which  $b = b_+ > 0$ . The “negative” solution  $b = b_-$  is the one which is relevant for rapidly rotating neutron stars, as shown in section 5.

vanishes. It can only reduce to other forms of nonrotating vacuum solutions (e.g. the well-known Weyl solutions) that could be matched to other interior solutions, such as nonrotating stars with non-isotropic stresses, inducing nonvanishing quadrupole deformations. Nevertheless, as we will show next, the analytic solution can approximately describe a rapidly rotating fluid star, when the rotation rate is large enough, so that the quadrupole deformation induced by the rotation roughly exceeds the minimum nonvanishing oblate quadrupole deformation of the solution in the absence of rotation, i.e. roughly when

$$|Q| > M^3/4. \quad (34)$$

Since the quadrupole moment is roughly proportional to  $a^2M$ , one expects that the analytic solution could be relevant for rotation rates of roughly  $j > 0.5$ , where  $j \equiv J/M^2$  is a dimensionless measure of the angular momentum of the star. We will confirm this expectation by direct comparisons with numerical solutions in the next section.

It is interesting that the Kerr solution can still be obtained from the analytic solution, if one accepts the following imaginary form for the parameter  $b$

$$b = i\sqrt{M^2 - a^2}, \quad (35)$$

with  $a \leq M$ . In this case, one recovers the correct expressions  $Q = -a^2M$  and  $S_3 = -a^3M$ .

#### 4 MATCHING THE INTERIOR AND EXTERIOR SOLUTIONS

The three parameters of the analytic solution ( $M, a$  and  $b$ ) can be set at will. However, only certain combinations of values can correspond to specific models of rapidly rotating neutron stars. Since the solution has four nonvanishing multipole moments, but only three free parameters, one can at most match three multipole moments of any given numerical solution. The fourth multipole moment will then be determined by the analytic solution, and its relative difference with the (known) numerical value will be a measure of the accuracy of the analytic solution. The four multipole moments are not equally important for specifying a solution,  $S_3$  being the least

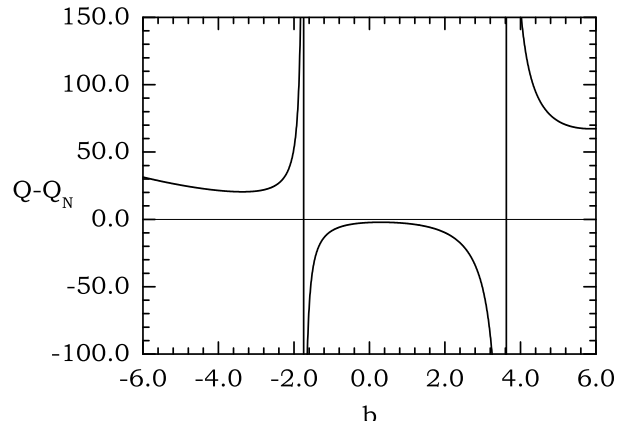


**Figure 3.** The matching condition  $Q - Q_N = 0$  as a function of  $b$  for a slowly rotating model in the maximum-mass sequence for EOS FPS (fourth row of  $M_B = 2.105M_\odot$  sequence in Table 3). No real solution exists.

important, even for the most rapidly rotating models. Therefore we choose to match the analytic exterior solution to known numerical solutions by matching the gravitational mass  $M$ , the specific angular momentum  $a$  and the mass-quadrupole moment  $Q$ . One then hopes that the resulting analytic solution will yield a value for the current-octupole moment  $S_3$  that is close to the corresponding value in the numerical model. As we will show, there exists a branch of solutions for which this is indeed the case. Manko *et al.* (2000a) also used the quadrupole moment to match numerical and analytic solutions, but their examples correspond to the other branch of solutions, for which the analytic value of  $S_3$  does not agree well with the numerical value.

For a given model of a rapidly rotating neutron star, we first construct a highly accurate numerical solution, as described in section 2. In the analytic solution (23), we set  $M$  and  $a$  to be equal to the obtained numerical values. The remaining parameter  $b$  is then determined by solving the equation

$$Q - Q_N = 0, \quad (36)$$

where  $Q_N$  is the value of the quadrupole moment obtained by the numerical code. A plot of  $Q - Q_N$  as a function of the parameter  $b$ , for the most rapidly rotating model of the maximum-mass sequence for EOS FPS, is shown in Fig. 2. Two possible real solutions for  $b$  exist: a solution that is usually negative,  $b_-$ , and a solution that is always positive,  $b_+$ . Thus, for each set of physical parameters  $M, a$  and  $Q$ , there exists two different branches of solutions, with parameters  $(M, a, b_-)$  and  $(M, a, b_+)$ , respectively. In the remainder of the paper, we will refer to these two different branches as the negative solution (-) and the positive solution (+). As we will show next, these two branches correspond to very different spacetimes.

In the previous section, we estimated that the analytic solution should be relevant for rapidly rotating neutron stars only for values of  $j$  roughly larger than 0.5. Fig. 3 shows a more slowly rotating model than the model shown in Fig. 2, along the same evolutionary sequence. It is obvious that no solution to equation (36) exists for any real value of the parameter  $b$ . Along each sequence there is a critical rotation rate above which one can match the numerical interior solution to the analytic exterior solution. In Tables (1–5) we list all computed physical properties for the selected sequences. The last column lists the parameter  $b = b_-$  of the *negative* branch of the analytic solution (when it exists). This is the relevant branch for rapidly rotating neutron stars, as we will show in section 5. In

Tables (1–5) some models appear having  $b = b_- > 0$ . These models do *not* belong to the positive branch  $b_+$ . They are instead models which are very close to the critical value of the rotation parameter,  $j = j_{crit}$ : in these particular cases, both solutions to equation (36) can happen to be positive. However, in general (as long as a model is rotating somewhat above the critical rate) the negative branch has  $b_- < 0$ .

Typical values of  $j_{crit}$  above which the analytic solution exists are listed in Table 6 for a subset of the considered EOSs. For smaller masses,  $j_{crit}$  is usually smaller: therefore, for “canonical” neutron stars (having mass  $M \sim 1.4M_\odot$  in the non rotating limit) the analytic solution is valid over a wider range of  $j$ . In terms of the angular velocity at the mass-shedding limit for uniformly rotating stars, the critical rotation rates are given in the right column of Table 6. The critical rotation rate  $\Omega_{crit}/\Omega_{Kepler}$  ranges from  $\sim 0.4$  to  $\sim 0.7$  for the  $M = 1.4M_\odot$  sequence, with the lower ratio corresponding to the stiffest EOS. For the maximum-mass sequence the ratio is  $\sim 0.9$ , nearly independent of the EOS. In conclusion, the analytic exterior solution can be useful for studying rapidly rotating neutron stars. The exterior gravitational field of massive neutron stars created in binary neutron star mergers, supported temporarily by differential rotation against collapse, could also be described, to some accuracy, by the analytic solution (the accuracy will depend on how significant the higher multipole moments are in the case of strong differential rotation). If the EOS is very stiff, such as EOS L, then the analytic solution is also valid for description of accreting neutron stars in Low-Mass-X-Ray binaries (LMXB), with rotational periods of a few milliseconds.

#### 4.1 Coordinate transformations between vacuum and non-vacuum metrics

Before presenting specific tests of the accuracy of the analytic solution, we need to describe the coordinate transformation that relates the interior metric (1) to the exterior *vacuum* metric (10) (see Islam 1985). For the interior metric (1), we define the cylindrical coordinates

$$\varpi \equiv r \sin \theta, \quad z \equiv r \cos \theta. \quad (37)$$

In vacuum, Einstein’s field equations imply that

$$\frac{\partial^2(\varpi B)}{\partial \varpi^2} + \frac{\partial^2(\varpi B)}{\partial z^2} = 0. \quad (38)$$

One can therefore define a new coordinate

$$\tilde{\rho} \equiv \varpi B, \quad (39)$$

satisfying the two-dimensional Laplace equation (38), and a second coordinate

$$\tilde{z} = \tilde{z}(\varpi, z), \quad (40)$$

satisfying the Cauchy-Riemann conditions

$$\frac{\partial \tilde{z}}{\partial \varpi} = -\frac{\partial \tilde{\rho}}{\partial z} = -\varpi \frac{\partial B}{\partial z}, \quad (41)$$

$$\frac{\partial \tilde{z}}{\partial z} = \frac{\partial \tilde{\rho}}{\partial \varpi} = B + \varpi \frac{\partial B}{\partial \varpi}. \quad (42)$$

The coordinate  $\tilde{z}$  is obtained by integration of the above Cauchy-Riemann conditions, requiring that  $\tilde{z} = 0$  in the equatorial plane (at  $z = 0$ ). It is easy to show that

$$d\varpi^2 + dz^2 = \left[ \left( \frac{\partial \tilde{\rho}}{\partial \varpi} \right)^2 + \left( \frac{\partial \tilde{z}}{\partial \varpi} \right)^2 \right]^{-1} (d\tilde{\rho}^2 + d\tilde{z}^2), \quad (43)$$

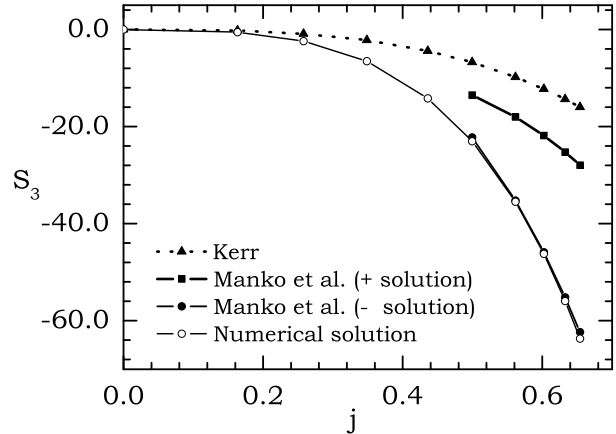


**Figure 4.** The current octupole moment  $S_3$  as a function of  $j$  for the numerical solution, for the Kerr metric, and for the negative and positive branches of the analytic solution. For illustrative purposes we have chosen the FPS EOS, and fixed our attention on the sequence having maximum mass in the non rotating limit. The negative branch reproduces with excellent accuracy the numerical behavior of the current octupole, so it is the branch appropriate for describing the exterior spacetime of rapidly rotating neutron stars.

and setting

$$f = e^{2\nu} - \omega^2 \tilde{\rho}^2 e^{-2\nu}, \quad (44)$$

$$w = -\frac{\omega \tilde{\rho}^2 e^{-2\nu}}{f}, \quad (45)$$

$$e^{2\gamma} = f \left[ \left( \frac{\partial \tilde{\rho}}{\partial \varpi} \right)^2 + \left( \frac{\partial \tilde{z}}{\partial \varpi} \right)^2 \right]^{-1} e^{2\alpha}, \quad (46)$$

the metric in the exterior takes the desired form (10). Since the transformation (41,42) for the coordinate  $\tilde{z}$  cannot, in general, be solved analytically, one can relate a solution for the interior metric (1) to the exterior metric (10) only through numerical integration.

## 5 TESTS OF THE ACCURACY OF THE ANALYTIC SOLUTION

### 5.1 The current-octupole moment

The current-octupole moment  $S_3$ , like the quadrupole moment  $Q \equiv M_2$ , is a function of  $a$ ,  $b$  and  $M$ . Once we have fixed  $b$  by matching the quadrupole moment to the numerical spacetime through equation (36), there are no more free parameters to be specified; the current-octupole  $S_3$  can be computed using equation (29), and then compared to the value of  $S_3$  computed for the numerical metric. Therefore,  $S_3$  serves as a good error indicator for the accuracy of the solution. In fact, the value of  $S_3$  obtained analytically for the two branches of solutions,  $b_+$  and  $b_-$ , can be used to distinguish which of the solutions is more relevant for rapidly rotating neutron stars. Fig. 4 displays  $S_3$ , for the two branches of the analytic solution, along with the value of  $S_3$  for the numerical solution and for the Kerr solution, for the evolutionary sequence corresponding to EOS FPS and having maximum mass in the nonrotating limit (see Table 3). The error for the (-) solution is very small, at most of the order of 3%. On the other hand the error for the (+) solution is quite large (up to 56% for the fastest rotating model). In this case the solution is closer to the Kerr value than to the value corresponding to numerical models of rapidly rotating neutron stars.

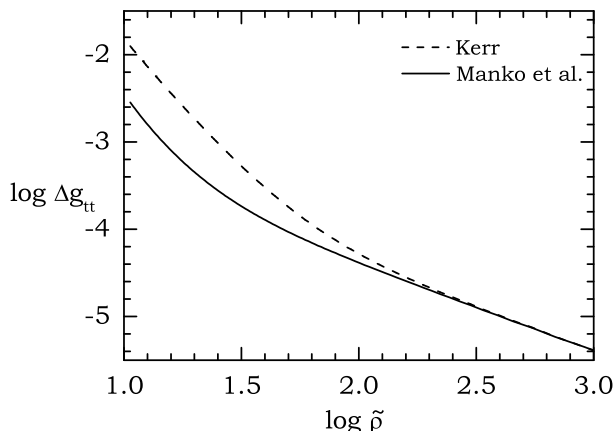


**Figure 5.** Relative error in the  $g_{tt}$ -component of the analytic metric and of the Kerr metric in the equatorial plane, when compared to the numerical solution for a rapidly rotating star.

Therefore, in the remainder of this paper we will only use the (-) branch of solutions to the matching condition (36).

In Table 7 we display the relative error  $\Delta S$  in the analytic value of  $S_3$  (when compared to the numerical solution) for the critically rotating and maximally rotating models of all evolutionary sequences considered in this paper. For most sequences, the relative error in  $S_3$  can be as large as 12% for the critically rotating models, reducing to a few percent only for the models at the mass-shedding limit. Typically, the largest errors appear for the  $1.4M_\odot$  sequences, while the sequences that terminate at the maximum mass static model have the smallest errors. In most cases the error is larger for slower rotating models. This shows that for those models  $S_3$  is still influenced by its nonzero value in the non rotating case (for the analytic solution, the octupole moment  $S_3$ , like the quadrupole moment  $Q$ , does not vanish for  $a = 0$  and  $b \neq 0$ ). For more rapidly rotating models this influence diminishes and  $S_3$  becomes almost entirely of rotational origin, agreeing better with the numerical solution. Comparing the various EOSs, one sees that the error in  $S_3$  for soft EOSs, such as EOS A, is smaller than the corresponding error for very stiff EOSs, such as EOS L. The critical  $1.4M_\odot$  model for EOS L shows an unusually large relative error of 45% in  $S_3$ . This, again, is related to the compactness of the various models and to the value of the multipole moments for  $a = 0$ .

## 5.2 Direct comparison of metric components

As a second test of the accuracy of the analytic solution for rapidly rotating neutron stars, we performed a direct comparison of specific metric components for several representative models, using all EOSs in our sample. Here, we focus on the most rapidly rotating model of the maximum mass sequence with EOS FPS, since the other cases we examined showed similar behavior.

For this model we computed the metric components  $g_{tt}$ ,  $g_{t\phi}$  and  $g_{\phi\phi}$  on the equatorial plane and along the symmetry axis using the analytic metric and the Kerr metric. Then we compared the relative error of both metrics with respect to the corresponding components of the numerical metric.

Fig. 5 shows the relative error of the  $g_{tt}$ -component of the analytic metric and of the Kerr metric in the equatorial plane. For the analytic metric the error is only 0.3% at the surface of the star (located at  $\tilde{r} = 10.6$ ), and decreases monotonically with increasing distance, becoming of order  $10^{-6}$  near infinity. In comparison,

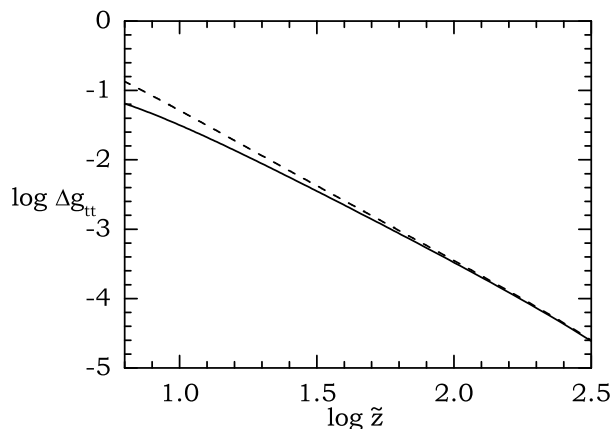


**Figure 6.** Same as Fig. 5, but along the axis of symmetry.

the relative difference between the Kerr metric and the numerical metric is 1.3% at the equator (i.e., four times larger than the error in the analytic metric). The relative difference between the Kerr metric and the numerical metric also decreases with increasing distance, as expected, and for distances larger than about 200 equatorial radii, the difference between the analytic solution and the Kerr solution is negligible. In other words, at such a distance the error in the analytic solution is dominated by the Kerr contribution at first order in the rotational parameter, while the effects of the higher-order multipole moments  $Q$  and  $S_3$  have become unimportant. The corresponding figure for the relative error in  $g_{\phi\phi}$  on the equatorial plane is nearly identical to Fig. 5 for  $g_{tt}$ . When we consider  $g_{t\phi}$  in the equatorial plane, the relative error at the surface is 1.3% for the analytic metric and 5.3% for the Kerr metric. This larger error for  $g_{t\phi}$  should be expected: this metric component vanishes in the non-rotating limit, so it is more sensitive to contributions by the higher-order multipole moments  $Q$  and  $S_3$  than the metric components  $g_{tt}$  and  $g_{\phi\phi}$ .

In order to compare the metric components on the symmetry axis, we first need to integrate the Cauchy-Riemann conditions (41) and obtain the coordinate  $\tilde{z}$  in terms of the coordinate  $z$ . This can be done easily, once the numerical solution for the metric function  $B$  is obtained. Fig. 6 shows the relative error in  $g_{tt}$  for the analytic solution and the Kerr solution along the symmetry axis. The location of the surface (as determined from the numerical solution) is at  $\tilde{z} = 6.05$ . At the surface, the relative error for the analytic solution is 7%, while it is 15% for the Kerr metric. Thus, we see that the effect of a large quadrupole moment  $Q$  shows up predominantly in the metric components along the symmetry axis, while in the equatorial plane this effect is very small. The reason for this difference is that a rapidly rotating star becomes very oblate, so that the stellar surface on the symmetry axis is located deeper in the gravitational potential well than the surface in the equatorial plane. The specific example shown in the above figures has polar to equatorial axes ratio of 0.6, thus the equatorial radius is roughly twice as large as the polar radius. The analytic value of  $g_{tt}$  on the surface in the equatorial plane is  $-0.59$ , while it is  $-0.44$  on the surface on the symmetry axis (the asymptotic value at large distances is  $-1$ ). Gravity is stronger on the polar surface, and this justifies a larger relative error in  $g_{tt}$  there. At about 3 polar radii, the relative error in  $g_{tt}$  along the symmetry axis decreases to the 1% level for both the analytic and Kerr solutions.

The above direct comparison of metric components shows that the analytic metric is a good approximation to the numerical one



(or, at least, a much better approximation than the Kerr metric) in the equatorial plane, where one expects particle orbits to be astrophysically more relevant. For gravitational-wave extraction in numerical relativity, the larger inaccuracies near the polar surface could influence the waveforms. In order to minimize this effect, the extraction should be done as far as possible from the surface of the star. In any case, the analytic metric is everywhere more accurate than the Kerr metric. Thus a perturbative wave-extraction scheme, built with the analytic metric as a background, should yield more accurate waveforms than those obtained with techniques available at present (which are based on a perturbative extraction of waveforms around a Schwarzschild or Kerr background).

### 5.3 Innermost stable circular orbits

It is well known that not all orbits around relativistic stars are stable. For nonrotating stars, the ISCO is located at a circumferential radius of  $R_{ISCO} = 6M$ . Depending on the EOS and the mass of the star, the ISCO can be located outside the stellar surface. Rotation introduces a preferred direction in the  $\phi$  coordinate, so ISCOs around a rotating star belong to two distinct families: a corotating and a counterrotating one. For moderate rotation rates, the effect of rotation is to shorten the distance between the surface and the corotating ISCO. For rapid rotation, the large quadrupole moment of the star reverses this trend (notice that even in some Newtonian stellar models, large higher-order multipole moments can introduce an ISCO (see, Zdzunik & Gourgoulhon, 2001; Amsterdamski *et al.* 2002)). The counterrotating ISCO radius normally increases with rotation. Detailed computations of ISCOs for a large number of models and EOSs are presented in CST; we also refer the reader to that paper for the equations defining the ISCOs that were used in our numerical computations.

Testing the accuracy of the analytic solution in computing the properties of ISCOs is important, as ISCOs are related to several astrophysical properties of rapidly rotating neutron stars in LMXBs. An accretion disk cannot extend to radii located within the ISCO, and this sets an upper limit to the Keplerian frequency of particles orbiting a star. This idea could be used, e.g., in determining whether compact stars in LMXBs are composed of strange matter (Stergioulas, Kluzniak & Bulik 1999, Gondek *et al.* 2001). In addition, the location of the ISCO could play a role in the mechanism producing the kHz quasi-periodic oscillations observed in many LMXBs (van der Klis 2000): see, e.g., Kluzniak *et al.* (2003).

A circular orbit in the equatorial plane is one for which  $\varpi = \text{const.}$ , and hence  $\tilde{\rho} = \text{const.}$  The equation for geodesic motion along the radial coordinate  $\tilde{\rho}$  reads

$$-g_{\tilde{\rho}\tilde{\rho}} \left( \frac{d\tilde{\rho}}{d\tau} \right)^2 = 1 - \frac{\mathbf{E}^2 g_{\phi\phi} + 2\mathbf{E}\mathbf{L}g_{t\phi} + \mathbf{L}^2 g_{tt}}{g_{\tilde{r}\tilde{r}}^2 - g_{tt}g_{\phi\phi}} \equiv V(\tilde{\rho}), \quad (47)$$

where  $\mathbf{E}$  and  $\mathbf{L}$  are the conserved energy and angular momentum per unit mass, determined by the conditions  $V = dV/d\tilde{\rho} = 0$ . Geodesics become unstable when  $d^2V/d\tilde{\rho}^2 = 0$ , or

$$\left( w' w'' f^5 \tilde{\rho} (2f - f' \tilde{\rho}) + w'^2 f^4 [2f^2 + (-f'^2 + f'' f) \tilde{\rho}^2] + w' f^2 \sqrt{w'^2 f^4 + f' \tilde{\rho} (2f - f' \tilde{\rho})} [2f^2 + 2f'^2 \tilde{\rho}^2 - f \tilde{\rho} (4f' + f'' \tilde{\rho})] + \tilde{\rho} (2f - f' \tilde{\rho}) \left\{ 3f' f^2 - 4f'^2 f \tilde{\rho} + f'^3 \tilde{\rho}^2 + f^2 [f'' \tilde{\rho} - w'' f \sqrt{w'^2 f^4 + f' \tilde{\rho} (2f - f' \tilde{\rho})}] \right\} \right) /$$

$$\left( f^2 \tilde{\rho}^2 \left\{ w'^2 f^4 + 3f' f \tilde{\rho} - f'^2 \tilde{\rho}^2 - f^2 [2 + w' \sqrt{w'^2 f^4 + f' \tilde{\rho} (2f - f' \tilde{\rho})}] \right\} \right) = 0 \quad (48)$$

for corotating orbits (cf. Stute & Camenzind, 2002), where  $'$  indicates a partial derivative with respect to  $\tilde{\rho}$ . For counter-rotating orbits, one can simply use the above equation and change the sign of the star's angular momentum.

Shibata & Sasaki have used a more general representation of axisymmetric vacuum solutions (in the form of a series expansion that is completely determined by the physical multipole moments of the spacetime: see Fodor, Hoenselaers and Perjés 1989 and Ryan 1995) and derived an approximate analytic formula for the location of the ISCO. Their formula depends on the stellar mass, angular momentum, mass quadrupole, current octupole and mass  $2^4$ -pole moments. Including all terms up to order  $O(4)$  in the rotation parameter, they find the following equation for the circumferential radius of the corotating ISCO:

$$\begin{aligned} R_{ISCO} &= 6M(1 - 0.54433j - 0.22619j^2 + 0.17989Q_2 \\ &- 0.23002j^3 + 0.26296jQ_2 - 0.05317q_3 \\ &- 0.29693j^4 + 0.44546j^2Q_2 - 0.06249Q_2^2 \\ &+ 0.01544Q_4 - 0.11310jq_3). \end{aligned} \quad (49)$$

In the previous expression we have introduced dimensionless parameters  $Q_2 = -Q/M^3$ ,  $q_3 = -S_3/M^4$  and  $Q_4 = M_4/M^5$ . In the case of the Kerr metric, the approximate expression for the location of the corotating ISCO up to order  $O(j^4)$  is (see, e.g., Shapiro & Teukolsky 1983)

$$\begin{aligned} R_{ISCO}^{Kerr} &= 6M(1 - 0.54433j - 0.04630j^2 \\ &- 0.02016j^3 - 0.01110j^4). \end{aligned} \quad (50)$$

The location of the counter-rotating ISCO is obtained from the above formulae by reversing the sign of  $j$  and  $S_3$ .

For illustrative purposes we again focus on the three sequences of EOS FPS (Table 3). We have carried out the calculation for other EOSs as well. Although there are quantitative differences between the various models, the qualitative behavior and the relative accuracy between the numerical and analytic solutions remain similar to those shown here.

For each sequence we find the relative error in computing corotating and counter-rotating ISCO radii with respect to the numerical solution. We perform this comparison for the analytic solution obtained through our matching procedure (when a solution to the matching condition exists), for the Shibata-Sasaki formula (49) and for the Kerr formula (50). In the case of the Shibata-Sasaki formula we do not explicitly compute the moment  $M_4$  from the numerical solution, but we follow the same approximation adopted by Shibata & Sasaki. Namely, we set  $Q_4 = \alpha_4 Q_2^2$ , where  $\alpha_4$  is expected to take values ranging between 0 and 2. Again, following Shibata & Sasaki, we normally set  $\alpha_4 = 1$  (unless otherwise noted).

Fig. 7 shows the relative errors in computing the ISCOs for the sequence having  $M = 1.4M_\odot$  in the non rotating limit. In this and in the following Figures, negative values of  $j$  correspond to counter-rotating orbits, while positive values of  $j$  correspond to corotating orbits. In the corotating case the ISCO disappears at slow rotation rates, even before the analytic solution becomes valid; therefore, for this sequence, we can only compare the accuracy in finding counter-rotating ISCOs. For the Kerr solution the error increases monotonically with  $|j|$ , reaching 11% for the fastest rotating model. On the other hand, the error for the Shibata-Sasaki formula with

$\alpha_4 = 1$  is only 2% for the fastest rotating model. For this sequence the analytic solution is initially close to the Shibata-Sasaki formula, but then shows a rather large error, that becomes 10% for the fastest rotating model. The explanation for this behavior is that at very large rotation rates the inclusion of the multipole moment  $M_4$  is important, but this multipole moment is absent in the analytic solution. When we omit  $M_4$  in the Shibata-Sasaki formula (while still keeping all other mixed terms up to order  $O(4)$ ) by setting  $\alpha_4 = 0$ , we obtain an error which is much closer to the error made using the analytic solution. On the other hand, including only terms up to  $O(3)$  in the Shibata-Sasaki formula gives a much smaller error, comparable to (or better than) the error of the formula when all orders up to  $O(4)$  with  $\alpha_4 = 1$  are included. What this comparison underlines is the importance of being consistent up to a certain order in the rotation parameter. The Shibata-Sasaki formula has small error when used consistently up to  $O(3)$  or up to  $O(4)$ , but a large error when only a few mixed terms up to  $O(4)$  are included. The error of the Shibata-Sasaki formula to order  $O(4)$  should improve, if one would include the precise values for  $M_4$ , instead of the crude estimate of  $\alpha_4 = 1$ . The analytic solution suffers from the inconsistency that while the  $M_4$  moment vanishes, it is still an exact analytic solution. This means that mixed terms containing  $j$ ,  $Q$  and  $S_3$  up to order  $O(4)$  are present. It follows that, for the counterrotating ISCOs in Fig. 7, the analytic solution is not as accurate as a consistent application of the Shibata-Sasaki formula. Notice that the non-monotonic increase in the error for the counter-rotating ISCO with the Shibata-Sasaki formula at large rotation rates is a consequence of the moment  $M_4$  becoming important near the mass-shedding limit: for sequences of larger mass, as the ones we examine next,  $M_4$  appears to be much less important.

The comparison of the error in computing the ISCOs is much more favorable for the analytic solution in the case of the other two sequences we examined. Fig. 8 shows the errors for the evolutionary sequence that terminates at the maximum-mass nonrotating model. In this case, a corotating ISCO exists for some models for which the analytic solution is valid. The error made with the analytic solution is 5% for the fastest rotating model, and it is consistently better than the error of the Shibata-Sasaki formula. For counter-rotating orbits the error for the analytic solution is somewhat smaller than for corotating orbits (which is expected, as the ISCO for corotating orbits is normally at larger radii). However, the error is consistently larger than the error of the Shibata-Sasaki formula. The corresponding errors for the supramassive sequence, shown in Fig. 9, are very similar to the errors for the sequence in Fig. 8.

#### 5.4 Comparison to other matching conditions

Manko *et al.* (2000a) also use the quadrupole moment  $Q$  in order to match the analytic solution to a numerical one. However, they redefine the parameter  $b$  as

$$b = \pm \sqrt{a^2 + 2aM\Delta - M^2}, \quad (51)$$

where  $\Delta$  is a new parameter, with the motivation that now  $\Delta$  measures the departure of the analytic solution from the Kerr metric. We find that the above redefinition is not necessary, as it does not change the solution: in other words, a solution with a given  $b$  has a corresponding value of  $\Delta$ . In Manko *et al.* (2000a) it is not mentioned that  $Q$  can be set to the numerical value only for a limited range of the parameter  $b$  (or, equivalently, of  $\Delta$ ). Moreover, we find that the illustrative solutions they give do *not* correspond to the

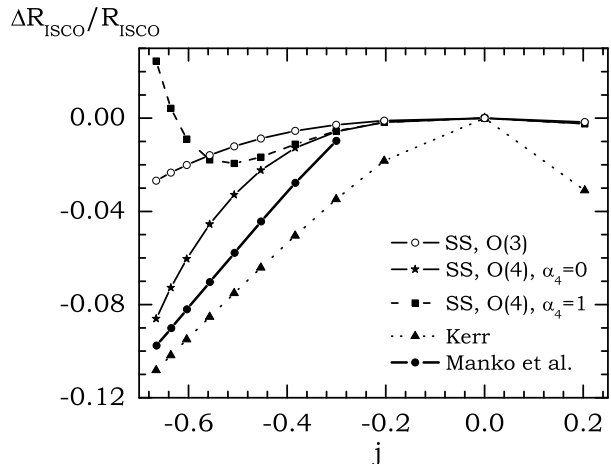


**Figure 7.** Errors in the ISCO for the EOS FPS sequence with constant rest mass corresponding to a nonrotating model of  $1.4 M_\odot$ . Negative values of  $j$  represent counterrotating orbits. The various curves are explained in the main text.

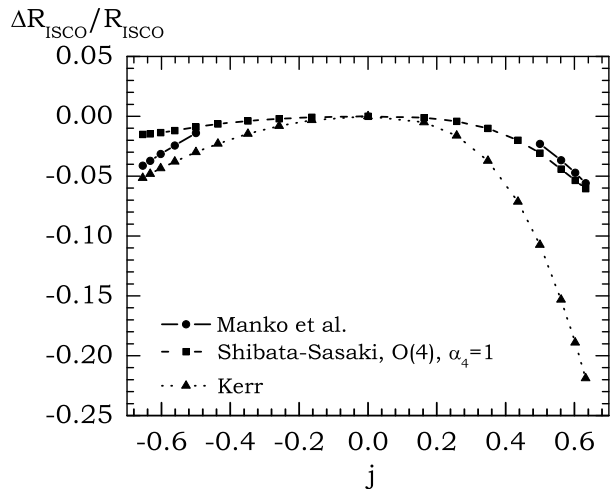


**Figure 8.** Similar to Fig. 7, for the EOS FPS sequence with constant rest mass corresponding to a nonrotating model of maximum mass.

negative branch of solutions for  $b$  (that, as we have seen, are those relevant for rapidly rotating stars) but rather to the positive branch, which is closer in behavior to the Kerr metric.

Stute & Camenzind (2002) fix the third parameter in the analytic solution,  $b$ , by matching the value of the metric function  $g_{tt}$  at the stellar equator. However, this is a local quantity, so that the analytic and numerical metrics are matched only at a single point in the  $(\tilde{\rho}, \tilde{z})$  plane. Experimenting with this choice, we found that one can obtain numerical solutions that are also limited to rapidly rotating stars. However, since the parameter  $b$  is not fixed directly, but only indirectly, one has to solve a nonlinear equation in order to obtain  $b$  for a given value of  $g_{tt}$  at the equator. This procedure could lead to multiple solutions, and one has to choose the one closest to a rapidly rotating neutron star by examining other properties of the spacetime (e.g. the higher multipole moments). As we have seen, fixing  $Q$  also leads to multiple solutions, however, we find that the procedure of fixing directly three leading multipole moments ( $M$ ,

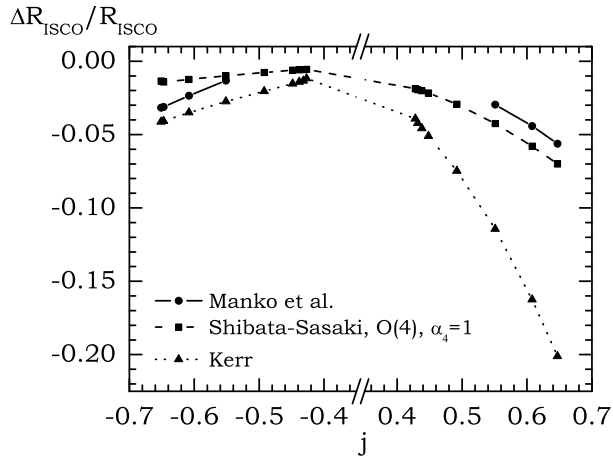


**Figure 9.** Similar to Fig. 7, for a supramassive EOS FPS sequence with constant rest mass.

$j$  and  $Q$ ) and selecting the desired solution according to the value of a fourth multipole moment ( $S_3$ ) is more intuitive than fixing  $M$ ,  $j$  and the value of a metric function at a single point in the spacetime.

In the matching procedure used by Stute & Camenzind the parameter  $b$  is not chosen to be real. They rather impose that  $b$  continuously reduces to the Schwarzschild value,  $b = iM$ , in the nonrotating limit ( $a \rightarrow 0$ ). However, the Schwarzschild and Kerr solutions can only (formally) be obtained as limiting cases of the Manko solution by analytic continuation in the complex- $b$  plane. In a sense, the black hole solutions are “isolated points” on the pure-imaginary axis of the complex- $b$  plane, while solutions representing neutron star exteriors lie on the pure-real axis. Therefore, the requirement imposed by Stute & Camenzind violates one of the original requirements of the analytic solution (namely, that all three parameters of the solution must be real). If one follows this procedure, the resulting metric components are, in general, complex. For complex values of  $b$  one could, in principle, use the real parts of some quantities in order to compute an estimate for the location of the ISCO, as was done by Stute & Camenzind. However, in such cases, even the coordinates in which the metric is expressed become complex numbers. Furthermore, additional multipole moments appear that are not present in the numerical solution, rendering the analytic solution inappropriate for describing the physical properties of a rotating neutron star.

Finally, an important point in the matching procedure is to use the correct correspondence between the coordinates in the analytic exterior spacetime (10) and the numerical spacetime (1). Stute & Camenzind transformed the analytic metric to Boyer-Lindquist like coordinates, but these are *not* the coordinates used in (1). This can easily be seen when one considers that the metric (1) reduces to the Schwarzschild metric in *isotropic* coordinates (not in the usual Schwarzschild coordinates) in the nonrotating limit.

## 6 CONCLUSIONS

We have investigated the properties of a closed-form analytic solution for the exterior spacetime of rapidly rotating neutron stars. We matched it to highly-accurate numerical solutions, imposing that the quadrupole moment of the numerical and analytic spacetimes be the same. For the analytic solution we considered, such a

matching condition can be satisfied only for very rapidly rotating stars. We found that solutions belong to two branches, only one of which is a good approximation to the exterior of rapidly rotating neutron star spacetimes. In order to evaluate the accuracy of the analytic solution in describing rapidly rotating neutron stars, we presented a comparison of the radii of ISCOs obtained with a) the analytic solution, b) the Kerr metric, c) an analytic series-expansion derived by Shibata & Sasaki and d) a highly-accurate numerical code. In most cases we found that the analytic solution has an accuracy consistently better than the Shibata-Sasaki expansion up to  $O(j^4)$ , for corotating orbits. Only for counterrotating orbits does the higher-order Shibata-Sasaki expansion perform better than the analytic solution. We have only shown direct comparisons for three constant rest-mass sequences and one representative EOS (FPS); however our qualitative conclusions also hold for other EOSs.

The analytic solution we studied in this paper could become useful in constructing outgoing-wave boundary conditions for simulations of pulsating relativistic stars, and for the computation of quasinormal modes of oscillation as an eigenvalue problem (a long-standing problem in relativistic astrophysics). Another potential application is the study of high-frequency variability in accretion disks around rapidly rotating relativistic stars. We emphasize, however, that this analytic solution is only valid for rapidly rotating stars, contrary to previous claims in the literature. For stars of intermediate rotation rates one can use the exterior analytic solution by Hartle & Thorne (1968), valid to second order in the rotation rate. This approximate solution is determined by the three multipole moments  $M$ ,  $j$  and  $Q$ , but higher-order multipole moments are ignored. It would be interesting to determine whether the region in which the second-order Hartle-Thorne metric is valid to some accuracy, overlaps with the region in which the analytic solution considered here is valid. Such a study, along with a characterization of the spacetimes using invariant quantities (constructed in the Newman-Penrose formalism) will be reported elsewhere (Berti *et al.*, in preparation).

## Acknowledgements

We wish to thank Marco Bruni, John L. Friedman, Kostas Kokkotas, Mina Maniopolou, Vladimir Manko, Masaru Shibata, Nail Sibgatullin, Frances White and Leszek Zdunik for useful discussions and correspondence. We are grateful to the anonymous referee for a very careful reading of the paper and many suggestions. This work has been supported by the EU Programme ‘Improving the Human Research Potential and the Socio-Economic Knowledge Base’ (Research Training Network Contract HPRN-CT-2000-00137).

## REFERENCES

- A. Abrahams, D. Bernstein, D. Hobill, E. Seidel, L. Smarr, 1992, *Phys. Rev. D*, 45, 3544.
- G. Allen, K. Camarda, E. Seidel, 1998, gr-qc/9806036.
- P. Amsterdamski, T. Bulik, D. Gondek-Rosinska, W. Kluzniak, 2002, *Astron. Astrophys.* 381, L21.
- A. Akmal, V. R. Pandharipande, D. G. Ravenhall, 1998, *Phys. Rev. C*, 58, 1804.
- J. Baker, M. Campanelli, 2000, *Phys. Rev. D*, 62, 127501.
- J. Baker, M. Campanelli, C. O. Lousto, 2002, *Phys. Rev. D*, 65, 044001.
- E. Berti, F. White, A. Maniopolou, M. Bruni, in preparation.
- G. B. Cook, S. L. Shapiro, S. A. Teukolsky, 1994, *ApJ*, 424, 823.
- F. J. Ernst, 1968, *Phys. Rev.*, 168, 1415.
- G. Fodor, C. Hoenselaers, Z. Perjés, 1989, *J. Math. Phys.* 30, 2252.

## 12 *Emanuele Berti and Nikolaos Stergioulas*

- D. Gondek-Rosinska, N. Stergioulas, T. Bulik, W. Kluzniak, E. Gourgoulhon, 2001, *Astron. Astrophys.* 380, 190.
- J. B. Hartle, 1968, *ApJ*, 150, 1005.
- J. B. Hartle, K. S. Thorne, 1968, *ApJ*, 153, 807.
- J. N. Islam, 1985, *Rotating fields in general relativity*, Cambridge University Press.
- W. Kluzniak, M. A. Abramowicz, S. Kato, W. H. Lee, N. Stergioulas, 2003, *astro-ph/0308035*.
- W. Kinnersley, D. M. Chitre, 1978, *J. Math. Phys.* 19, 10.
- H. Komatsu, Y. Eriguchi, I. Hachisu, 1989, *MNRAS*, 237, 355.
- W. G. Laarakkers, E. Poisson, 1999, *ApJ*, 512, 282.
- V. S. Manko, J. Martín, E. Ruiz, 1995, *J. Math. Phys.* 36, 3063.
- V. S. Manko, E. W. Mielke, J. D. Sanabria-Gómez, 2000a, *Phys. Rev. D* 61, 081501(R).
- V. S. Manko, J. D. Sanabria-Gómez, O. V. Manko, 2000b, *Phys. Rev. D* 62, 044048.
- V. S. Manko, N. R. Sibgatullin, 1993, *CQG* 10, 1383.
- T. Nozawa, N. Stergioulas, E. Gourgoulhon, Y. Eriguchi, 1998, *Astron. Astrophys. Suppl. Ser.* 132, 431.
- A. Papapetrou, 1953, *Ann. Phys.* 12, 309.
- F. D. Ryan, 1995, *Phys. Rev. D* 52, 5707.
- F. D. Ryan, 1997, *Phys. Rev. D* 55, 6081.
- M. E. Rupright, A. M. Abrahams, L. Rezzolla, 1998, *Phys. Rev. D*, 58, 044005.
- S. L. Shapiro, S. A. Teukolsky, 1983, *Black holes, white dwarfs, and neutron stars*, Wiley, New York, Chap. 12.
- M. Shibata, M. Sasaki, 1998, *Phys. Rev. D* 58, 104011.
- N. R. Sibgatullin, 1991, *Oscillations and waves in strong gravitational and electromagnetic fields* (Engl. transl.), Springer, Berlin [orig. Russian, 1984, Nauka, Moscow].
- N. R. Sibgatullin, R. A. Sunyaev, 1998, *Astronomy Letters* 24, 774.
- N. R. Sibgatullin, R. A. Sunyaev, 2000, *Astronomy Letters* 26, 699.
- N. R. Sibgatullin, 2002, *Astronomy Letters* 28, 83.
- N. Stergioulas *Rotating Stars in Relativity*, *Living Reviews in Relativity*, 2003.
- N. Stergioulas, J. A. Font, 2001, *Phys. Rev. Lett.* 86, 1148.
- N. Stergioulas, J. L. Friedman, 1998, *Astrophys. J.* 492, 301.
- N. Stergioulas, W. Kluzniak, T. Bulik, 1999, *Astron. Astrophys.* 352, L116.
- M. Stute, M. Camenzind, 2002, *MNRAS* 336, 831.
- M. van der Klis, 2000, *Ann. Rev. of Astron. Astrophys.* 38, 717.
- J. L. Zdunik, E. Gourgoulhon, 2001, *Phys. Rev. D* 63, 087501.

$\epsilon_c$ $10^{15} \text{ g cm}^{-3}$	$\Omega$ $10^3 \text{ s}^{-1}$	$I$ $10^{45} \text{ g cm}^2$	$M$ $M_\odot$	$T/W$ -	$R_e$ km	$h_+$ km	$h_-$ km	$M_2$ $\text{km}^3$	$J$ $\text{km}^2$	$S_3$ $\text{km}^4$	$b$ km
$M_B = 1.589M_\odot$											
1.8582	0.000	-	1.402	0.0000	9.570	2.841	2.841	0.000	0.0000	0.000	-
1.8127	3.205	1.023	1.405	0.0099	9.741	1.609	4.115	-1.001	0.8121	-0.727	-
1.7422	5.005	1.070	1.410	0.0257	10.04	0.924	4.866	-2.656	1.327	-3.158	-
1.6744	6.138	1.121	1.415	0.0411	10.36	0.485	5.354	-4.377	1.704	-6.694	-0.4777
1.6093	6.952	1.174	1.419	0.0563	10.71	0.151	5.706	-6.173	2.022	-11.23	-0.6302
1.5467	7.565	1.232	1.424	0.0712	11.12	-	5.951	-8.063	2.307	-16.77	-0.6738
1.4939	7.982	1.285	1.428	0.0840	11.53	-	6.073	-9.806	2.540	-22.50	-0.6701
1.4502	8.266	1.333	1.432	0.0948	11.97	-	6.083	-11.37	2.729	-28.10	-0.6486
1.4146	8.463	1.376	1.435	0.1038	12.46	-	5.961	-12.74	2.884	-33.35	-0.6214
1.4050	8.511	1.388	1.435	0.1062	12.64	-	5.883	-13.13	2.925	-34.88	-0.6128
$M_B = 1.948M_\odot$											
4.1300	0.000	-	1.658	0.0000	8.362	6.313	6.313	0.000	0.0000	0.000	-
3.4156	3.571	1.115	1.662	0.0734	8.740	4.701	7.315	-0.623	0.9857	-0.376	-
3.0643	5.410	1.174	1.668	0.0186	9.042	3.776	7.897	-1.657	1.573	-1.637	-
2.7492	6.942	1.249	1.676	0.0341	9.419	2.911	8.422	-3.237	2.147	-4.459	-
2.4664	8.172	1.343	1.686	0.0533	9.894	2.104	8.883	-5.434	2.717	-9.667	-
2.2736	8.893	1.427	1.694	0.0696	10.34	1.540	9.163	-7.529	3.143	-15.72	-0.2679
2.1245	9.371	1.509	1.701	0.0842	10.79	1.081	9.336	-9.619	3.501	-22.64	-0.4798
2.0123	9.595	1.576	1.708	0.0945	11.20	0.723	9.356	-11.31	3.746	-28.76	-0.5568
1.9060	9.852	1.660	1.714	0.1078	11.79	0.252	9.309	-13.52	4.051	-37.53	-0.5941
1.8500	10.00	1.715	1.719	0.1163	12.38	-	9.092	-15.03	4.247	-44.00	-0.5972
$M_B = 2.038M_\odot$											
3.8786	8.671	1.210	1.742	0.0416	8.892	3.443	9.917	-3.489	2.598	-4.943	-
3.7154	8.603	1.227	1.742	0.0423	8.977	3.363	9.867	-3.615	2.614	-5.221	-
3.5592	8.597	1.246	1.743	0.0436	9.071	3.255	9.840	-3.809	2.653	-5.654	-
3.4095	8.646	1.267	1.744	0.0457	9.175	3.123	9.836	-4.077	2.714	-6.266	-
3.2660	8.742	1.291	1.745	0.0485	9.291	2.967	9.853	-4.423	2.796	-7.082	-
2.9334	9.123	1.361	1.751	0.0583	9.633	2.499	9.963	-5.653	3.076	-10.24	-
2.4701	9.866	1.513	1.765	0.0817	10.40	1.593	10.22	-8.890	3.697	-20.13	-0.2083
2.2667	10.19	1.611	1.773	0.0964	10.94	1.077	10.29	-11.21	4.064	-28.43	-0.4423
2.1252	10.37	1.697	1.780	0.1086	11.51	0.606	10.24	-13.32	4.361	-36.78	-0.5274
2.0800	10.42	1.728	1.782	0.1128	11.76	0.401	10.16	-14.09	4.462	-40.03	-0.5443

**Table 1.** Equilibrium properties for three sequences of constant rest mass  $M_B$ , constructed with EOS A. We show a sequence that corresponds to a gravitational mass of  $M = 1.4M_\odot$  in the nonrotating limit ( $M_B = 1.589M_\odot$ ), a sequence that terminates at the maximum-mass nonrotating model in the nonrotating limit ( $M_B = 1.948M_\odot$ ) and a supramassive sequence ( $M_B = 2.038M_\odot$ ).

$\epsilon_c$ $10^{15} \text{ g cm}^{-3}$	$\Omega$ $10^3 \text{ s}^{-1}$	$I$ $10^{45} \text{ g cm}^2$	$M$ $M_\odot$	$T/W$ —	$R_e$ km	$h_+$ km	$h_-$ km	$M_2$ $\text{km}^3$	$J$ $\text{km}^2$	$S_3$ $\text{km}^4$	$b$ km
$M_B = 1.578M_\odot$											
1.2062	0.000	—	1.402	0.0000	10.39	2.020	2.020	0.000	0.0000	0.000	—
1.1922	2.951	1.191	1.405	0.0111	10.57	0.796	3.452	-1.416	0.8704	-1.126	—
1.1728	4.431	1.235	1.409	0.0262	10.84	0.277	4.228	-3.364	1.355	-4.168	-0.3280
1.1483	5.618	1.292	1.415	0.0446	11.20	—	4.867	-5.818	1.798	-9.564	-0.6683
1.1296	6.276	1.339	1.418	0.0582	11.51	—	5.214	-7.703	2.081	-14.66	-0.7247
1.1112	6.789	1.386	1.422	0.0712	11.85	—	5.462	-9.581	2.331	-20.44	-0.7266
1.0931	7.196	1.435	1.426	0.0836	12.24	—	5.615	-11.46	2.558	-26.87	-0.7019
1.0779	7.478	1.479	1.429	0.0938	12.63	—	5.655	-13.08	2.739	-32.87	-0.6691
1.0628	7.708	1.522	1.431	0.1035	13.13	—	5.562	-14.68	2.906	-39.20	-0.6305
1.0580	7.772	1.536	1.432	0.1065	13.34	—	5.479	-15.19	2.957	-41.32	-0.6173
$M_B = 2.636M_\odot$											
3.0200	0.000	—	2.136	0.0000	9.405	9.507	9.507	0.000	0.000	0.000	—
2.5479	3.765	2.080	2.145	0.0098	9.739	7.269	11.26	-1.370	1.939	-1.031	—
2.3008	5.831	2.173	2.158	0.0256	10.04	5.935	12.32	-3.701	3.138	-4.622	—
2.1014	7.384	2.283	2.174	0.0447	10.39	4.822	13.18	-6.740	4.176	-11.44	—
1.9411	8.503	2.402	2.190	0.0645	10.78	3.916	13.85	-10.14	5.059	-21.24	—
1.8135	9.298	2.526	2.205	0.0836	11.19	3.166	14.36	-13.72	5.817	-33.57	—
1.7136	9.847	2.651	2.219	0.1010	11.62	2.541	14.71	-17.30	6.465	-47.71	—
1.6377	10.20	2.766	2.231	0.1156	12.07	2.016	14.91	-20.58	6.986	-62.16	-0.1302
1.5829	10.41	2.865	2.240	0.1271	12.53	1.553	14.96	-23.37	7.389	-75.49	-0.3222
1.5327	10.57	2.970	2.249	0.1382	13.34	0.793	14.64	-26.32	7.778	-90.56	-0.4275
$M_B = 2.799M_\odot$											
2.7800	9.849	2.401	2.297	0.0682	10.16	4.647	15.80	-10.16	5.856	-19.56	—
2.7266	9.815	2.413	2.297	0.0686	10.20	4.614	15.77	-10.28	5.865	-19.95	—
2.6250	9.783	2.439	2.298	0.0699	10.28	4.526	15.75	-10.59	5.909	-20.99	—
2.5271	9.802	2.470	2.300	0.0721	10.38	4.403	15.76	-11.06	5.995	-22.55	—
2.2982	9.991	2.562	2.308	0.0807	10.67	3.979	15.87	-12.85	6.339	-28.61	—
2.0900	10.35	2.688	2.320	0.0946	11.07	3.390	16.12	-15.74	6.886	-39.28	—
1.9372	10.66	2.814	2.333	0.1085	11.48	2.836	16.33	-18.87	7.427	-52.04	—
1.8299	10.88	2.928	2.344	0.1207	11.90	2.351	16.46	-21.80	7.888	-65.12	—
1.7285	11.06	3.066	2.357	0.1343	12.51	1.721	16.46	-25.39	8.400	-82.46	0.0939
1.6800	11.14	3.145	2.364	0.1416	13.15	1.108	16.15	-27.46	8.674	-93.17	-0.1280

**Table 2.** Same as Table 1, but for EOS AU.

$\epsilon_c$ $10^{15} \text{ g cm}^{-3}$	$\Omega$ $10^3 \text{ s}^{-1}$	$I$ $10^{45} \text{ g cm}^2$	$M$ $M_\odot$	$T/W$ —	$R_e$ km	$h_+$ km	$h_-$ km	$M_2$ $\text{km}^3$	$J$ $\text{km}^2$	$S_3$ $\text{km}^4$	$b$ km
$M_B = 1.561M_\odot$											
1.2974	0.000	—	1.402	0.0000	10.85	1.560	1.560	0.000	0.000	0.000	—
1.2660	2.844	1.238	1.404	0.0111	11.07	0.312	2.970	-1.512	0.872	-1.241	—
1.2303	4.076	1.285	1.408	0.0238	11.35	—	3.622	-3.312	1.297	-4.051	-0.3392
1.1908	5.012	1.341	1.412	0.0382	11.70	—	4.129	-5.417	1.665	-8.518	-0.6669
1.1525	5.696	1.401	1.415	0.0523	12.09	—	4.493	-7.598	1.977	-14.21	-0.7508
1.1201	6.159	1.456	1.419	0.0643	12.48	—	4.715	-9.573	2.222	-20.16	-0.7596
1.0885	6.532	1.515	1.422	0.0763	12.92	—	4.846	-11.64	2.451	-27.10	-0.7381
1.0578	6.831	1.577	1.425	0.0881	13.48	—	4.847	-13.79	2.668	-35.06	-0.6986
1.0364	7.007	1.624	1.428	0.0964	14.02	—	4.699	-15.40	2.819	-41.46	-0.6629
1.0157	7.150	1.672	1.430	0.1044	15.05	—	4.049	-17.02	2.961	-48.26	-0.6244
$M_B = 2.105M_\odot$											
3.3900	0.000	—	1.802	0.0000	9.276	6.674	6.674	0.000	0.000	0.000	—
2.7939	3.204	1.462	1.806	0.0073	9.708	4.911	7.741	-0.830	1.160	-0.556	—
2.5016	4.833	1.543	1.813	0.0184	10.05	3.904	8.350	-2.200	1.847	-2.402	—
2.2399	6.184	1.645	1.821	0.0337	10.49	2.961	8.900	-4.303	2.519	-6.549	—
2.0056	7.260	1.772	1.831	0.0525	11.03	2.087	9.374	-7.222	3.185	-14.18	—
1.8461	7.887	1.885	1.840	0.0685	11.53	1.477	9.659	-10.01	3.683	-23.05	-0.3792
1.6992	8.370	2.017	1.849	0.0856	12.16	0.881	9.846	-13.37	4.181	-35.48	-0.5965
1.6079	8.613	2.117	1.855	0.0976	12.70	0.449	9.867	-15.97	4.515	-46.22	-0.6566
1.5426	8.760	2.199	1.860	0.1069	13.24	0.035	9.759	-18.16	4.771	-55.96	-0.6736
1.5000	8.846	2.260	1.864	0.1135	13.82	—	9.492	-19.80	4.951	-63.67	-0.6739
$M_B = 2.226M_\odot$											
3.2103	8.452	1.628	1.914	0.0492	9.977	3.346	11.04	-5.570	3.409	-9.594	—
3.0701	8.350	1.652	1.914	0.0496	10.07	3.268	10.96	-5.733	3.417	-10.03	—
2.9361	8.301	1.679	1.915	0.0507	10.18	3.163	10.92	-5.991	3.452	-10.72	—
2.8079	8.284	1.709	1.916	0.0524	10.30	3.035	10.88	-6.328	3.506	-11.64	—
2.6854	8.326	1.742	1.918	0.0550	10.44	2.875	10.88	-6.802	3.593	-12.98	—
2.3488	8.607	1.864	1.925	0.0665	10.94	2.279	10.96	-8.917	3.973	-19.46	—
2.0544	8.973	2.024	1.936	0.0833	11.62	1.554	11.08	-12.24	4.498	-31.21	-0.3080
1.8375	9.239	2.193	1.946	0.1007	12.45	0.831	11.07	-16.13	5.018	-47.06	-0.5536
1.7185	9.377	2.318	1.954	0.1131	13.27	0.162	10.83	-19.18	5.383	-60.96	-0.6168
1.6800	9.333	2.346	1.955	0.1145	13.56	—	10.60	-19.76	5.423	-63.67	-0.6293

Table 3. Same as Table 1, but for EOS FPS.

$\epsilon_c$ $10^{15} \text{ g cm}^{-3}$	$\Omega$ $10^3 \text{ s}^{-1}$	$I$ $10^{45} \text{ g cm}^2$	$M$ $M_\odot$	$T/W$ —	$R_e$ km	$h_+$ km	$h_-$ km	$M_2$ $\text{km}^3$	$J$ $\text{km}^2$	$S_3$ $\text{km}^4$	$b$ km
$M_B = 1.510M_\odot$											
0.4326	0.000	—	1.402	0.0000	14.83	—	—	0.000	0.0000	0.000	—
0.4266	1.816	2.162	1.404	0.0124	15.14	—	—	-3.671	0.9726	-3.554	-0.5958
0.4188	2.690	2.253	1.407	0.0286	15.58	—	0.541	-8.464	1.501	-12.65	-0.9422
0.4111	3.268	2.346	1.410	0.0443	16.06	—	1.283	-13.20	1.899	-24.96	-0.9455
0.4045	3.648	2.431	1.412	0.0577	16.52	—	1.749	-17.29	2.196	-37.84	-0.8901
0.3980	3.954	2.519	1.415	0.0709	17.05	—	2.077	-21.42	2.466	-52.65	-0.8151
0.3916	4.204	2.611	1.417	0.0839	17.68	—	2.250	-25.60	2.719	-69.47	-0.7311
0.3853	4.407	2.707	1.420	0.0965	18.49	—	2.195	-29.80	2.955	-88.00	-0.6444
0.3800	4.552	2.793	1.421	0.1070	19.61	—	1.693	-33.46	3.148	-105.4	-0.5693
0.3790	4.573	2.807	1.422	0.1087	19.97	—	1.430	-34.06	3.179	-108.4	-0.5569
$M_B = 3.232M_\odot$											
1.4700	0.000	—	2.713	0.0000	13.71	10.31	10.31	0.000	0.0000	0.000	—
1.2010	2.063	5.009	2.720	0.0069	14.20	7.868	12.01	-2.656	2.559	-2.558	—
1.0639	3.339	5.273	2.731	0.0200	14.65	6.260	13.22	-8.015	4.361	-13.43	—
0.9552	4.343	5.591	2.746	0.0372	15.19	4.888	14.27	-15.78	6.014	-37.00	—
0.8692	5.088	5.948	2.762	0.0564	15.80	3.767	15.14	-25.24	7.496	-74.63	—
0.8017	5.608	6.320	2.778	0.0752	16.45	2.889	15.80	-35.49	8.777	-124.1	-0.5411
0.7495	5.964	6.692	2.793	0.0927	17.14	2.189	16.28	-45.99	9.885	-182.6	-0.8287
0.7101	6.192	7.037	2.806	0.1077	17.82	1.623	16.56	-55.82	10.79	-243.8	-0.9222
0.6729	6.371	7.431	2.820	0.1234	18.73	0.958	16.65	-67.15	11.73	-321.3	-0.9373
0.6600	6.423	7.586	2.825	0.1293	19.19	0.628	16.57	-71.63	12.07	-353.8	-0.9275
$M_B = 3.470M_\odot$											
1.3847	6.095	5.855	2.929	0.0607	14.86	5.000	17.96	-24.16	8.839	-69.25	—
1.3199	6.030	5.927	2.929	0.0610	14.97	4.927	17.88	-24.68	8.851	-71.55	—
1.2500	5.994	6.021	2.931	0.0623	15.12	4.793	17.83	-25.72	8.938	-76.10	—
1.1992	5.993	6.103	2.932	0.0640	15.24	4.657	17.83	-26.85	9.058	-81.19	—
1.1160	6.042	6.268	2.937	0.0685	15.50	4.349	17.89	-29.62	9.381	-94.07	—
0.9665	6.282	6.712	2.952	0.0835	16.22	3.499	18.21	-38.85	10.44	-141.1	0.1274
0.8781	6.493	7.115	2.967	0.0981	16.90	2.791	18.51	-48.44	11.45	-196.2	-0.5157
0.8172	6.639	7.482	2.980	0.1111	17.56	2.199	18.70	-57.65	12.30	-254.4	-0.7332
0.7604	6.764	7.927	2.995	0.1261	18.49	1.463	18.75	-69.21	13.28	-334.2	-0.8412
0.7580	6.769	7.948	2.996	0.1268	18.54	1.423	18.74	-69.78	13.32	-338.4	-0.8437

**Table 4.** Same as Table 1, but for EOS L.



$\epsilon_c$ $10^{15} \text{ g cm}^{-3}$	$\Omega$ $10^3 \text{ s}^{-1}$	$I$ $10^{45} \text{ g cm}^2$	$M$ $M_\odot$	$T/W$ -	$R_e$ km	$h_+$ km	$h_-$ km	$M_2$ $\text{km}^3$	$J$ $\text{km}^2$	$S_3$ $\text{km}^4$	$b$ km
$M_B = 1.551M_\odot$											
0.9950	0.000	-	1.403	0.0000	11.55	0.874	8.737	0.000	0.0000	0.000	-
0.9800	2.756	1.368	1.407	0.0124	11.81	-	2.425	-1.965	0.9349	-1.750	-
0.9700	3.481	1.396	1.409	0.0202	11.99	-	2.856	-3.203	1.203	-3.673	-0.3370
0.9600	4.045	1.425	1.411	0.0280	12.18	-	3.195	-4.464	1.428	-6.064	-0.6044
0.9500	4.506	1.455	1.412	0.0356	12.37	-	3.470	-5.723	1.624	-8.852	-0.7155
0.9400	4.896	1.486	1.414	0.0432	12.58	-	3.699	-7.002	1.802	-12.03	-0.7689
0.9200	5.523	1.551	1.418	0.0581	13.05	-	4.036	-9.608	2.121	-19.50	-0.7935
0.9000	6.007	1.621	1.422	0.0727	13.62	-	4.209	-12.31	2.411	-28.49	-0.7644
0.8800	6.383	1.696	1.426	0.0870	14.41	-	4.129	-15.14	2.681	-39.17	-0.7089
0.8700	6.541	1.737	1.428	0.0943	15.04	-	3.855	-16.64	2.814	-45.32	-0.6744
$M_B = 2.672M_\odot$											
2.6000	0.000	-	2.205	0.0000	10.12	9.404	9.404	0.000	0.000	0.000	-
2.4500	2.820	2.298	2.212	0.0059	10.28	7.707	10.92	-0.905	1.605	-0.526	-
2.3000	3.828	2.352	2.217	0.0115	10.45	6.983	11.42	-1.846	2.230	-1.606	-
2.1000	5.360	2.451	2.228	0.0244	10.77	5.835	12.24	-4.059	3.254	-5.299	-
1.9000	6.791	2.593	2.243	0.0432	11.21	4.628	13.06	-7.604	4.362	-13.71	-
1.8000	7.465	2.687	2.253	0.0555	11.50	3.990	13.48	-10.06	4.967	-20.93	-
1.7000	8.066	2.799	2.263	0.0693	11.86	3.343	13.86	-13.07	5.592	-31.10	-
1.6000	8.605	2.939	2.276	0.0853	12.33	2.660	14.19	-16.82	6.263	-45.57	-
1.5000	9.048	3.113	2.290	0.1032	12.97	1.909	14.42	-21.52	6.977	-66.31	-0.2276
1.4000	9.384	3.337	2.307	0.1233	14.17	0.767	14.21	-27.54	7.756	-96.55	-0.5089
$M_B = 2.800M_\odot$											
2.5000	8.310	2.612	2.335	0.0540	10.75	4.968	15.03	-9.015	5.377	-16.70	-
2.4000	8.310	2.647	2.336	0.0556	10.86	4.841	15.02	-9.418	5.447	-17.93	-
2.3000	8.342	2.686	2.338	0.0579	10.99	4.679	15.01	-9.976	5.549	-19.68	-
2.2000	8.457	2.734	2.342	0.0617	11.13	4.450	15.07	-10.82	5.726	-22.32	-
2.1000	8.596	2.791	2.346	0.0664	11.30	4.185	15.15	-11.91	5.942	-25.97	-
2.0000	8.799	2.860	2.351	0.0728	11.52	3.850	15.27	-13.39	6.233	-31.09	-
1.9000	9.023	2.943	2.358	0.0807	11.78	3.467	15.40	-15.26	6.577	-38.03	-
1.8000	9.258	3.044	2.367	0.0901	12.10	3.030	15.55	-17.62	6.979	-47.47	-
1.7000	9.494	3.168	2.377	0.1013	12.52	2.521	15.68	-20.64	7.449	-60.54	-
1.6000	9.705	3.321	2.388	0.1143	13.11	1.894	15.72	-24.45	7.983	-78.60	0.0123

Table 5. Same as Table 1, but for EOS APRb.

EOS(sequence)	$j_{crit}$	$\Omega_{crit}/\Omega_{Kepler}$
A(1.44)	0.39	0.72
A(MM)	0.50	0.89
FPS(1.44)	0.30	0.57
FPS(MM)	0.50	0.89
L(1.44)	0.23	0.40
L(MM)	0.52	0.87

**Table 6.** Minimum (critical) rotation parameter  $j_{crit}$  and corresponding ratio of critical angular velocity  $\Omega_{crit}$  to Keplerian angular velocity  $\Omega_{Kepler}$ , for which the matching condition (36) has a real solution.

EOS(sequence)	$\Delta S_{crit}$	$\Delta S_{Kepler}$
A(1.44)	-11%	-4%
A(MM)	-5%	-2%
A(SM)	-2%	-4%
AU(1.44)	-11%	-5%
AU(MM)	-9%	-7%
AU(SM)	-11%	-10%
FPS(1.44)	-11%	-4%
FPS(MM)	-3%	-2%
FPS(SM)	-7%	-4%
L(1.44)	-45%	-4%
L(MM)	-3%	-2%
L(SM)	-12%	-4%
APRb(1.4)	-13%	-6%
APRb(MM)	-8%	-6%
APRb(SM)	-11%	-11%

**Table 7.** Relative difference in  $S_3$  between the negative branch of analytic solutions and the numerical solution, for different EOSs and evolutionary sequences. The difference is tabulated for the minimum (critical) rotation rate for which a real analytic solution exists ( $\Delta S_{crit}$ ) and for the model at the mass-shedding limit ( $\Delta S_{Kepler}$ ).